Lattice Bending in Electrooptically Active Poly(nonylbithiazole) and Poly(nonylbisoxazole)

Lebzylisbeth González-Ronda† and David C. Martin*

Macromolecular Science and Engineering Center and Department of Materials Science and Engineering, University of Michigan, Ann Arbor, Michigan 48109-2136

Received September 9, 2002; Revised Manuscript Received January 15, 2004

ABSTRACT: The ~2.4 nm (100) lattice planes of electrooptically active poly(nonylbithiazole) (PNBT) and poly(nonylbisoxazole) (PNBO) crystallites have been imaged by means of low-dose high-resolution transmission electron microscopy (HRTEM). The average dimensions of the observed crystallites were $(14 \pm 9) \times (13 \pm 6)$ nm (width vs length) and $(80 \pm 36) \times (22 \pm 9)$ nm for PNBT and PNBO, respectively. Atomization of dilute polymer solutions led to the formation of discontinuous thin films containing numerous holes. The influence of these surfaces on the crystallization process was evident in the preferential parallel orientation of the (100) fringes with respect to the film edges. Evidence of considerable lattice bending about the [010] ($\pi-\pi$ stacking) direction was observed in both compounds. Two-dimensional maps of the local lattice curvature revealed substantial differences in the modes of deformation of the two polymers: PNBT crystallites curved in a continuous fashion, whereas PNBO crystallites localized the distortions. Possible factors that could influence the observed deformation mechanisms are discussed.

Introduction

Curvature at the molecular level plays a prominent role in the morphology of fullerenes, micelles, vesicles, and many biological systems.[1] Determining the mechanisms by which thin films conform to curved surfaces is necessary to understand their properties and self-assembly behavior. Lattice bending has been recently observed in π-conjugated polymers and is expected to have a large impact on the performance of these materials in electrical and optical devices.[2,3] Distortions along the chain backbone have been found to strongly affect charge mobility along and between π-conjugated molecules,[4,5] while conformational changes resulting from solvent interactions and thermal mobility may lead to interesting optical changes.[6,7]

The mechanisms that give rise to lattice curvature are fairly well established for inorganic materials. In the absence of an applied stress, lattice curvature in plastically bent thin films is mediated by the presence of dislocations.[8] Thin films will initially contain more dislocations than necessary to accommodate the distortion.[9] Annealing leads to the annihilation of dislocations of opposite signs, while the remaining dislocations will be energetically driven to form grain boundaries.[9,10] The transition between undislocated and dislocated films has been proposed to be dependent on the elastic constant of the material, the film thickness, and its curvature.[10] For anisotropic solids, weak interplanar bonding may result in interlayer sliding and a decrease in the critical curvature or thickness. The degree to which layers slide with respect to each other will depend on the value of the stacking fault energy relative to the elastic modulus.[11]

Lattice curvature in polymeric materials is expected to be influenced by additional factors. Grain boundaries have been observed to mediate the local curvature of the (001) planes of the polyimide PMDA-12C in a manner similar to that previously observed in inorganic materials.[12] The presence of grain boundaries, however, should be affected by the molecular weight of the polymer. A lower molecular weight would increase the number of chain ends available to migrate to grain boundaries and lower their energy of formation.[12] The energetics and mobility of defects in polymers differ significantly from those observed in atomic solids because of the large influence of the covalently bonded chain.[13]

Lovinger and co-workers[14] have reported evidence of lattice curvature in a π-conjugated, high charge mobility organic material. High-resolution transmission electron microscopy (HRTEM) studies of the 3.6 nm (001) molecular length spacing of α,ω-dihexyl-α-hexathiophene (DHa6T) showed a curved morphology that appeared to extend throughout the entire film. Curvature radii as small as 20 nm were observed along with the presence of numerous dislocations and grain boundaries. The molecules were oriented side-on, with both the chain axis and the $\pi-\pi$ stacking direction parallel to the substrate. Thus, bending of the (001) planes likely resulted from sliding between (020) planes and the formation of lateral grain boundaries. Electron diffraction studies have shown persistent splay and warp along the 0.39 nm (020) planes of α-hexathienyl (a-6T).[15] Given the similarities between the crystal structures of the unsubstituted (a-6T) and end-substituted (DHa6T) thiophene hexamers, this deformation mechanism would also be likely to occur in DHa6T. Despite the low molecular weight of the molecules, the impact of chain ends on the deformation mode of DHa6T is expected to be minimized by their molecular orientation.

The molecular arrangement observed by Lovinger[14] for bent DHa6T crystallites differs from that previously reported for DHa6T by Garnier[15] and those of other candidate materials for thin film transistors (TFTs). Many oligomeric π-conjugated molecules, including unsubstituted thiophenes,[15−17] anthradithiophenes,[18] pentacene,[19,20] and metallophthalocyanines,[21] orient with the chain axis perpendicular, and the $\pi-\pi$ stacking

† Current address: Department of Materials Science, Ford Scientific Research Laboratory, Dearborn, MI 48121-2053.
* Corresponding author.

10.1021/ma025657e CCC: $27.50 © 2004 American Chemical Society
Published on Web 03/16/2004

direction parallel, to the substrate. Diffraction studies of poly(nonylbithiazole) (PNBT) single crystals have shown the chain axis to orient parallel to the substrate, with the $\pi-\pi$ stacking direction at varying angles with respect to the substrate.[22]

This paper reports the lattice bending of the (100) planes of π-conjugated poly(nonylbithiazole) (PNBT) and poly(nonylbisoxazole) (PNBO). Despite their similarities in chemical structure and molecular packing, PNBT and PNBO show significant differences in their optoelectronic behavior.[23−25] For example, the effective conjugation length and observed color of PNBT can vary with its degree of crystallinity, a behavior that is absent in PNBO. The following is an analysis of previously observed lattice curvature in PNBT[26] as compared to new evidence of this deformation in PNBO. A method for quantitatively characterizing the curvature deformation shown in HRTEM images is described, followed by a discussion of the mechanisms of deformation and the main factors expected to influence them. Quantitative, one-dimensional analyses of curvature have been previously performed using level set methods[27] to characterize the relaxation mechanisms of disclination loops.[28,29] Here, geometrical calculations are used to produce two-dimensional maps of local curvature to enable the assessment of the spatial arrangement of the deformation.

Experimental Procedure

Sample Preparation. 0.01 wt % solutions of nonylbithiazole trimer (NBT_3) and polymer (PNBT), both in chloroform, and poly(nonylbisoxazole) (PNBO) in tetrachloroethane were filtered through 0.45 mm Millipore membranes and atomized over carbon-coated mica sheets. The NBT_3-, PNBT-, and PNBO-coated mica sheets were then annealed at 90, 220, and 200 °C, respectively. The coated carbon films were removed from the mica by submerging the sheets into deionized water. TEM specimens were prepared by lifting the floating films with 400 mesh copper grids and allowed to air-dry overnight.

Imaging Conditions. A JEOL 4000EX operated at either 350 or 400 kV was used for low-dose HREM analysis of the annealed PNBT and PNBO samples. Conditions for searching, focusing, and photographing the samples were preset using a minimum dose system.[30] The critical dose (J_c) was experimentally estimated to be 0.018 C/cm^2 for NBT_3 and PNBT and 0.093 C/cm^2 PNBO. J_c was calculated to be 0.013 C/cm^2 for PNBT and 0.036 C/cm^2 for PNBO from the empirical relationship by Kumar and Adams that correlates a polymer's beam damage resistance to its melting or degradation temperature.[31] Successful HRTEM imaging was achieved with a magnification of 30 000×, a beam current of 8−13 pA/cm^2, and an exposure time of 1.0 s. The optimum defocus conditions for imaging the (100) lattice fringes were calculated from the relationship

$$\Delta f = \frac{d^2}{2\lambda} \tag{1}$$

where d is the lattice spacing of the material imaged and λ is the electron wavelength.[30] The lattice spacings were calibrated using a He−Ne optical bench and lattice images of graphitized carbon black (d = 0.34 nm).

Image Simulations. Multislice calculations were performed using the HRTEM module available with the Cerius^2 v3.5 software package[32] and the proposed structures for PNBT and PNBO.[22] The (100) fringes were simulated with the electron beam parallel to the [010] axis and the optimum defocus conditions described above. The spherical aberration coefficient and condenser aperture radius of the microscope have been previously determined to be 0.82 mm and 0.083 Å^{-1}.[33]

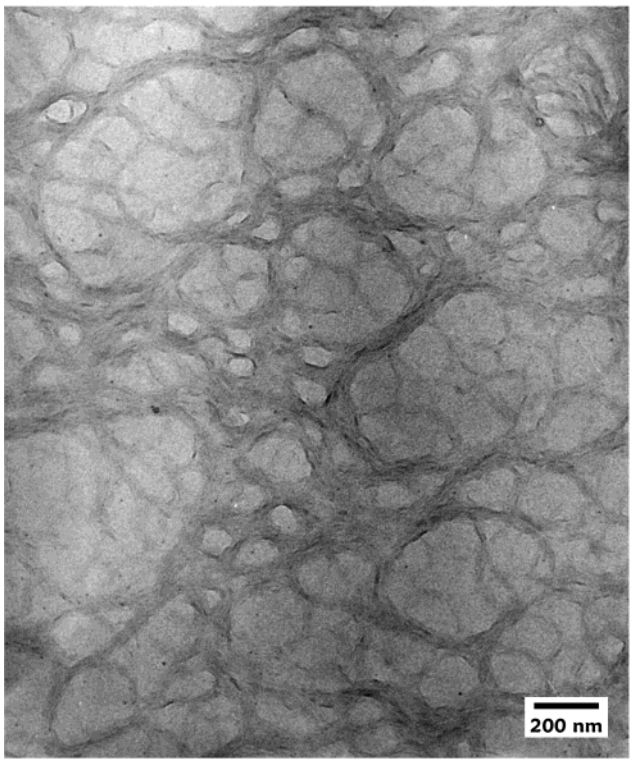

Figure 1. Bright field transmission electron microscopy (TEM) image of PNBT.

Image Analysis. The size, shape, and internal perfection of the imaged crystallite domains were determined by visual inspection, as has been described elsewhere.[12] Crystallite dimensions were measured along the main chain axis (parallel to the (100) fringes) and in the lateral packing direction (perpendicular to the (100) fringes). Crystallite orientation was determined relative to the nearest edge, evident as a slight variation in contrast relative to the carbon substrate.

The internal distortions of the crystallites were quantified with the aid of the public domain software NIH Image (available at http://rsb.info.nih.gov/nih-image/). We developed a macro for the NIH Image program that measures the local curvature radius of individual crystallites and creates a color-coded curvature map (see Supporting Information). The algorithm slices each fringe along its length, records the coordinates for the center of each resulting segment, calculates the radius of curvature over a user-specified length, and then colors each segment according to the curvature calculated at each point. Curvature maps were calculated for scales ranging from 2 to 22 nm by varying both the length of the segments into which a fringe was divided (1−2 nm) and the spacing between the segments used to calculate curvature (1−10 segments). The accuracy of the calculations was significantly improved by increasing image contrast through careful fast Fourier transform (FFT) filtering[34] using algorithms available with the NIH Image software.

Results

The annealed polymer samples formed discontinuous, rough films that contained numerous holes. Figures 1 and 2 show micrographs of typical PNBT films taken under bright field and high-resolution TEM imaging conditions, respectively. While bright field contrast emphasizes thickness and density variations across the sample, high-resolution (phase) contrast provides information about local variations in electron potential. Careful inspection of Figure 2 shows lattice fringes for the 2.4 nm spacing of PNBT, which corresponds to the long side-to-side intermolecular distance, or (100)

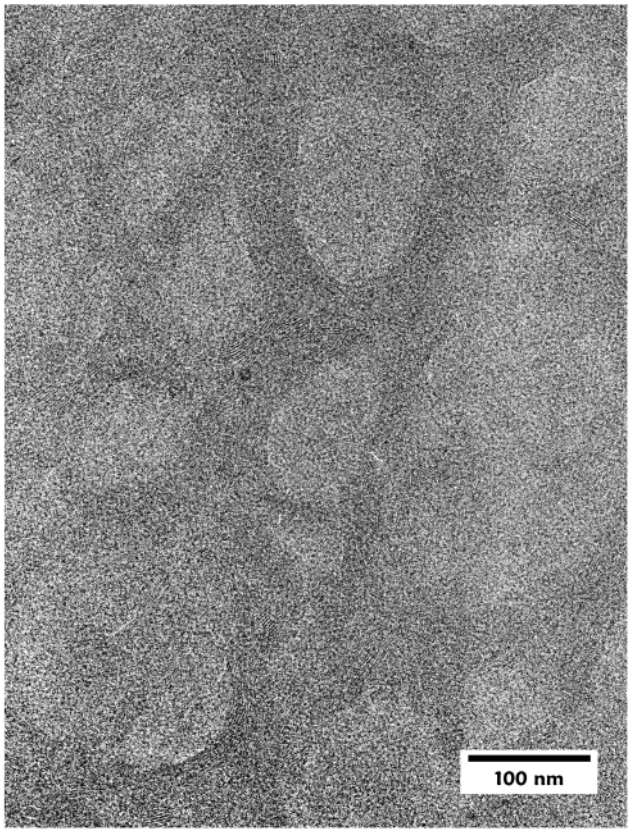

Figure 2. Low-magnification micrograph of PNBT obtained using high-resolution transmission electron microscopy (HRTEM) imaging conditions.

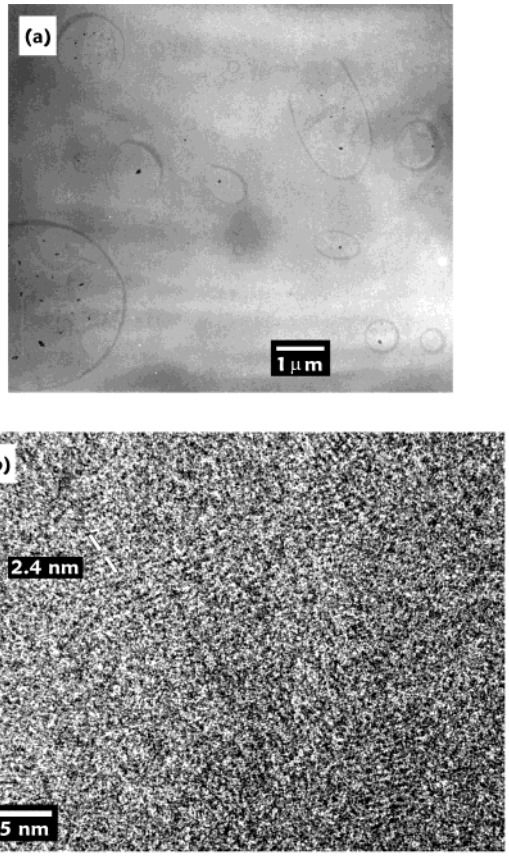

Figure 3. (a) Bright field transmission electron microscopy (TEM) image of NBT_3 samples. (b) HRTEM image of the (100) lattice fringes of NBT_3 ($d = 2.4$ nm).

planes.[24] The fringes are most evident near the edges of holes and tend to orient parallel to them. In contrast, the annealed NBT_3 samples formed droplets. Although contrast variations inside the droplets suggest a nonuniform topography, there was no evidence of discontinuities or holes within them (Figure 3).

Multislice calculations predict the (100) HRTEM fringes to run parallel to the polymer chain, where the $\pi-\pi$ stacking direction is perpendicular to the plane of the image. The imaging conditions used are expected to result in positive phase contrast, in which areas of higher projected electron potential—such as the molecular backbone—give rise to dark fringes on the image. The average projected crystallite dimensions along, and perpendicular to, the (100) fringes of NBT_3, PNBT, and PNBO are listed in Table 1. The size distributions of the crystallites are shown in Figure 4. Length refers to the direction parallel to the fringes, while width refers to the direction perpendicular to them. Also shown in Table 1 are the aspect ratios, or the ratio of average crystallite width to length, for NBT_3, PNBT, and PNBO crystals. PNBO crystals were found to have both larger average crystallite dimensions and a larger aspect ratio.

Evidence of considerable lattice bending about the [010] direction was obtained for both PNBT and PNBO (Figures 2, 5, and 6). In cases where both lattice fringes and the larger-scale topography of the sample were imaged, bent crystallites were most commonly observed near hole edges (Figure 2). Qualitative analysis of the HRTEM images revealed a difference in the mode of bending of the two materials. Bent PNBT crystallites curved almost exclusively in a continuous fashion (Figure 6), while bent PNBO crystals showed regions of high localized curvature, contrast discontinuities, and/or grain boundaries (Figure 5). Quantitative analysis of the local lattice curvature aided in distinguishing different bending modes by enabling the measurement of curvature at varying length scales. Examples of this approach are shown in Figures 7 and 8 for PNBT and PNBO crystallites, respectively. Each figure shows the HRTEM image of a bent crystallite (a), its curvature ($1/R_c$) maps and histograms for two different measurement length scales (labeled b and c, respectively), and its change in characteristic radius of curvature (R_c) as a function of length scale (d). The PNBT crystallite in Figure 7 shows a fairly uniform distribution of curvature for the two measurement length scales shown, while the PNBO crystallite in Figure 8 shows an area of localized curvature whose size and shape varies with measurement length scale. The characteristic curvature radii for the PNBT crystallite shown are 38 nm over a 4 nm length scale and 46 nm over a 7 nm length scale (Figure 7). The characteristic curvature radii for the PNBO crystallite shown are 33 nm over a 4 nm length scale and 29 and 53 nm over a 8 nm length scale (Figure 8). In both cases, R_c gradually increases with measurement length scale for short length scales and converges to larger values for longer length scales. The presence of localized bending in the PNBO crystallite shown in Figure 8 results in two characteristic radii.

Table 1. Average Crystallite Dimensions of NBT_3, PNBT, and PNBO Crystallites

	width (nm)	length (nm)	*W*/*L*
NBT_3	29 ± 15	15 ± 10	1.9
NBT_3	29 ± 15	15 ± 10	1.9
PNBT	14 ± 9	13 ± 6	1.1
PNBO	80 ± 36	22 ± 9	3.6

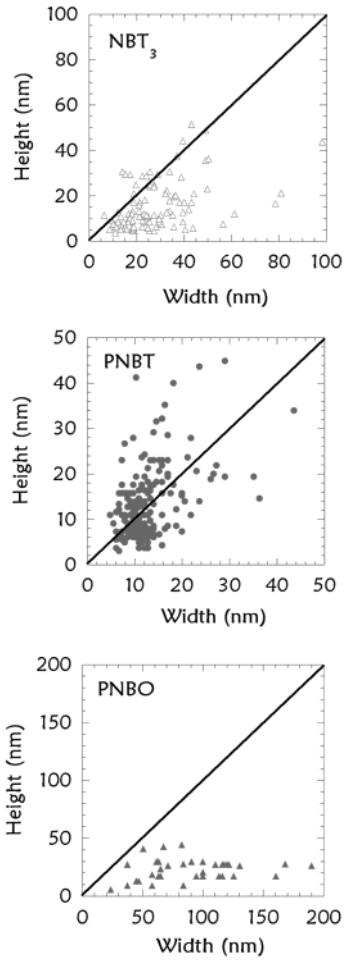

Figure 4. Distribution of the projected crystallite dimensions of NBT_3, PNBT, and PNBO. Lengths and widths were measured parallel and perpendicular to the (100) fringes, respectively.

Evidence of less dramatic lattice curvature was observed in the NBT_3 images, yet the surface constraints induced by the NBT_3 droplet morphology appeared to be weaker than those present in the polymer samples (Figure 3). Continuous deformation of the (100) fringes appeared to be the dominant bending mechanism, although delocalized deformation was also observed.

Discussion

The bending of the crystal lattices in PNBT and PNBO can be interpreted to be the combined result of surface constraints, surface energy considerations, and dislocation formation and motion. Crystallites near the hole edges preferentially align with the polymer chains parallel to the edge rather than expose the surface of chain ends and/or folds. Thus, during crystal growth chains prefer to conform to the curved surfaces of the discontinuous films, as has been previously observed for films of α,ω-dihexyl-α-hexathiophene (DHa6T)[3] and droplets of the polydiacetylene 1,6-di(*N*-carbazolyl)-2,4-hexadiyne (pDCHD).[2] However, the manner in which these molecules accommodate the deformation is fundamentally different (Figure 9). PNBT, like pDCHD, undergoes a continuous deformation that is presumably mediated by a uniform array of [001] dislocations.[8,9] PNBO, on the other hand, appears to rely heavily on axial chain rotation (ACR) grain boundaries to accommodate the distortion, and so it is said to deform discontinuously. Mediation of crystal deformation in polymers through ACR grain boundaries has been previously observed in the compression-induced kink bands of poly(*p*-phenylene benzobisoxazole) (PBZO or PBO).[35]

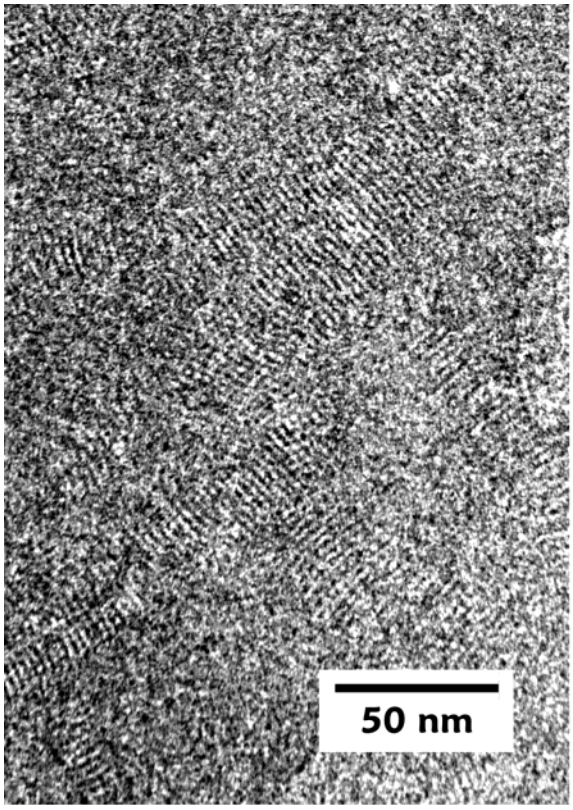

Figure 5. HRTEM image of the (100) lattice fringes of PNBO (d = 2.7 nm).

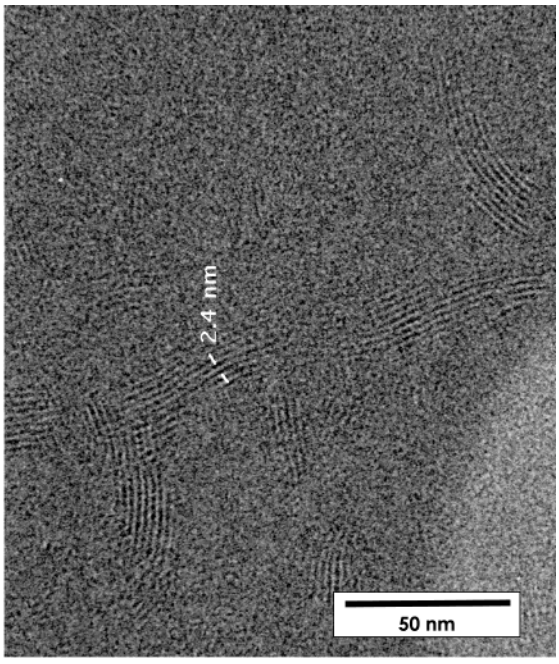

Figure 6. HRTEM image of the (100) lattice fringes of PNBT (d = 2.4 nm).

Some of the factors that may influence the manner in which polymers accommodate lattice bending include sample preparation and annealing, molecular weight effects, and molecular stiffness. For example, the de-

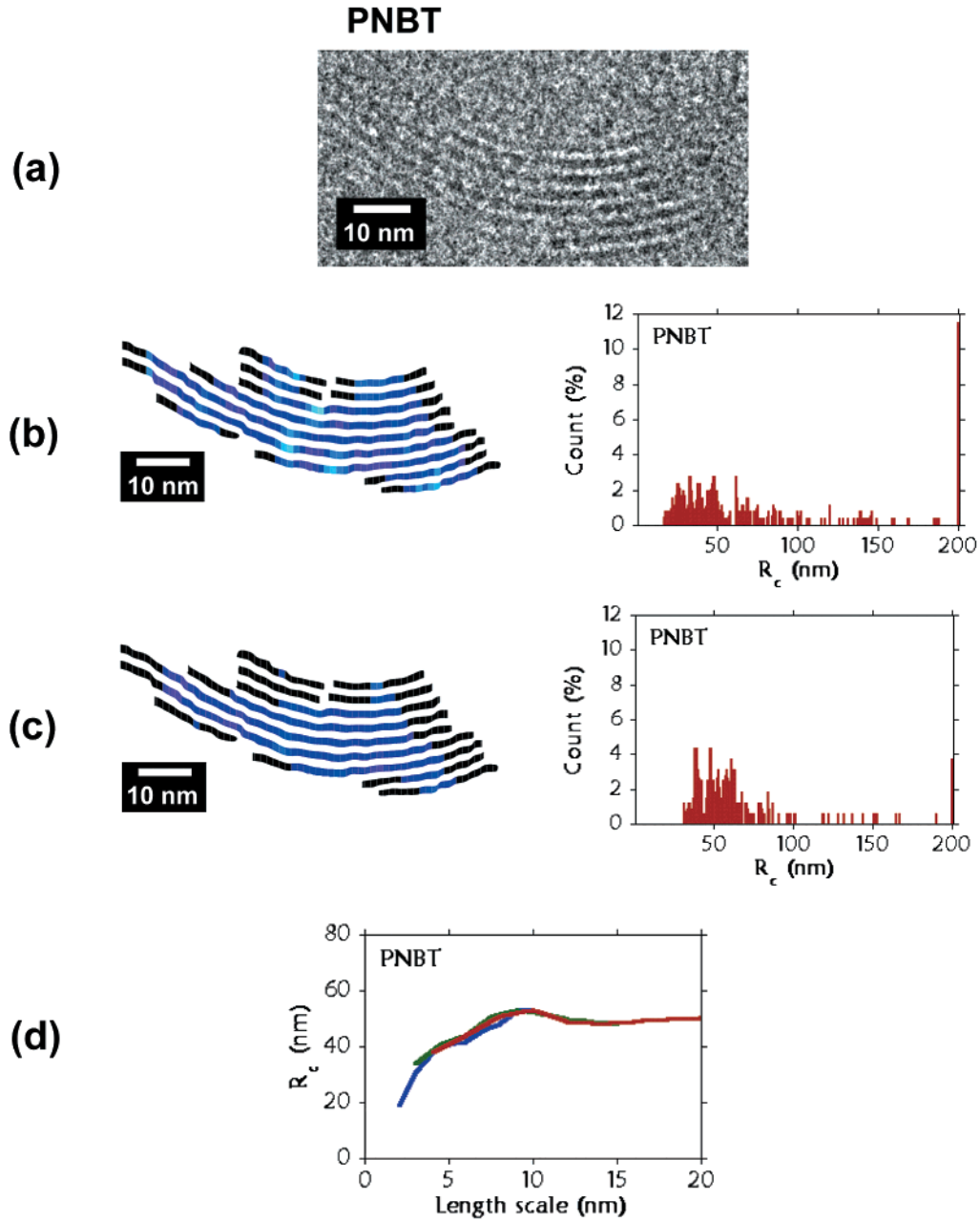

Figure 7. Example of continuous bending in PNBT crystallites: (a) HRTEM image of a bent crystallite, calculated curvature map for (b) 4 nm and (c) 7 nm, and (d) change in the characteristic curvature radii as a function of length scale.

formation of thin films undergoing small curvatures may be elastic, whereas thicker or more curved samples favor the formation of a uniform array of dislocations.[10,36] Differences in the crystallization conditions during sample preparation may promote or hinder the development of grain boundaries, which are expected to further lower the energy cost of bending.[9,10] The creation of grain boundaries might also be eased by chain end segregation, which in turn is influenced by the chain end density, i.e., the molecular weight of the sample.[12] Finally, molecular rigidity, or a larger bending constant, is expected to increase the critical curvature at which dislocations form and thus impact the mode of deformation observed.[36]

It is difficult to evaluate the individual contribution of these factors to the deformation behavior observed in PNBT and PNBO. Determining the influence of annealing conditions on grain boundary formation, for example, would require more detailed studies of the crystallization kinetics of both materials. Likewise, an assessment of the role of molecular weight in grain boundary formation necessitates a systematic study of molecules with varying chain lengths. The data presented here for NBT_3 appear somewhat inconclusive in this respect because of the differences in surface constraints in the oligomer and polymer samples. Surface constraints similar to those of the polymer samples have been observed in images of the 3.6 nm (001) fringes of α,ω-dihexyl-α-hexathiophene (DHa6T), an end-substituted thiophene hexamer.[3] However, the DHa6T molecules differ from PNBT and PNBO in their orientation and would require the presence of a different deformation mechanism. On the other hand, molecular mechanics simulations of the nonylbithiazole and nonylbisoxazole backbones have predicted some significant differences in the polymers' bending constants.[22] The PNBO backbone was calculated to have a persistence length (L_p) of 27 nm, while L_p was calculated to be 16

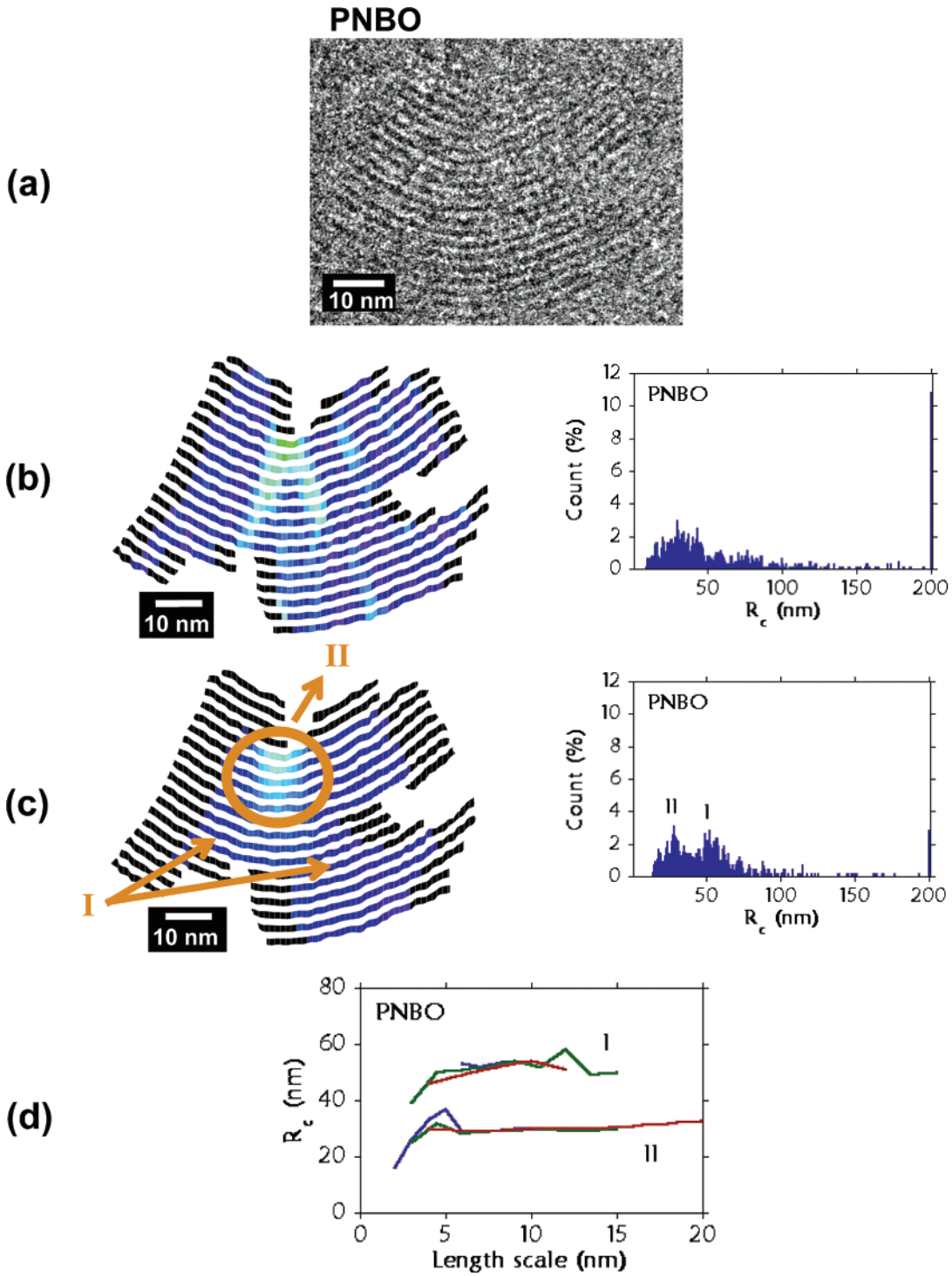

Figure 8. Example of mixed continuous and discontinuous bending in PNBO crystallites: (a) HRTEM image of a bent crystallite, calculated curvature map for (b) 4 nm and (c) 8 nm, and (d) change in the characteristic curvature radii as a function of length scale.

nm for PNBT. These calculations are consistent with experimental optical spectroscopy studies of NBO and NBT oligomers in which NBO oligomers were found to be more rigid in solution than NBT oligomers.[37]

Our analysis has shown the lattice curvature to be dependent on the length scale of the measurement. This dependence appears to have a more significant impact on the curvature localization shown by curvature maps than on the characteristic curvature values obtained from histograms (Figure 9). Figure 9 shows how the size and shape of high-curvature areas may differ at length scales for which the characteristic curvatures are quite similar. The discrepancy is consistent with the differences between the information that can be obtained from curvature maps and histograms. Curvature maps provide information regarding the spatial arrangement of the deformation and thus aid in distinguishing between continuous and discontinuous bending mechanisms. Meanwhile, a statistical evaluation of the calculated curvature values may aid in identifying periodicity, or even self-similarity, in the lattice deformation behavior. Self-similarity in a one-dimensional curve has been previously studied in the context of issues such as the surveying of natural shorelines.[38]

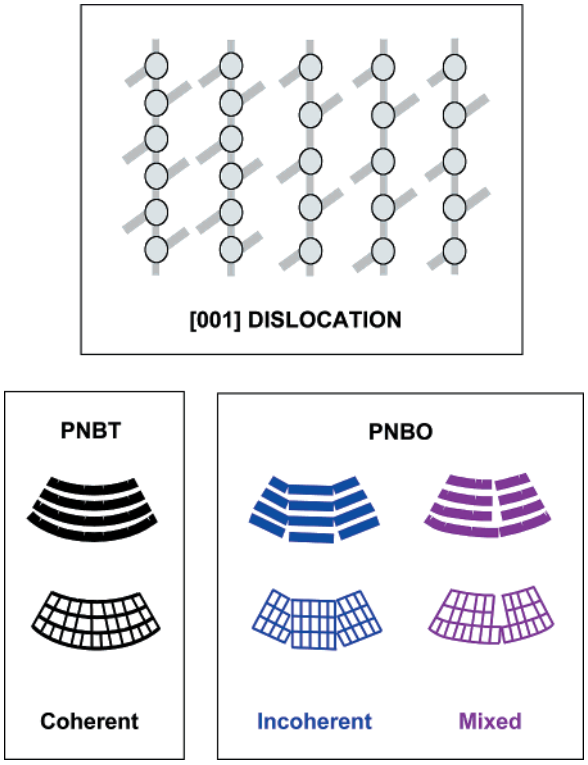

Figure 9. Schematic of various modes of bending observed in PNBT and PNBO HRTEM images.

An understanding of curvature variations as a function of length scale is necessary to define the nature of the lattice deformation. The importance of length scale dependence has been recognized for surface roughness,[39] and its characterization has been found relevant to issues as varied as biocompatibility[40] and ion implantation in silicon.[39] In the case of lattice curvature, length scale dependence might arise from scale-dependent variations in molecular stiffness. Variations of this type have been observed in Monte Carlo simulations of bottlebrush-shaped polymers, where chains were observed to be flexible locally but rigid at a molecular scale.[41] Although the discrepancies were evident by visual inspection, quantitative evaluation of the persistence length did not accurately describe chain stiffness at both length scales. Clearly, there is a need to establish better quantitative descriptions of molecular conformation that account for the scale of the measurement.

Conclusions

Bending of the (100) lattice planes was observed in high-resolution transmission electron microscopy (HRTEM) images of poly(nonylbithiazole) (PNBT) and poly(nonylbisoxazole) (PNBO). Despite the similarities in their chemical structure, the two polymers accommodate the deformation very differently. PNBT undergoes continuous deformation mediated by a distribution of [001] dislocations, while PNBO undergoes discontinuous deformation mediated by the presence of grain boundaries. Characterization of the deformation using curvature maps revealed the size and shape of the distortions to be dependent on the length scale at which curvature was measured. Such information was used to distinguish between continuous and discontinuous deformation modes. The mechanism of deformation is believed to be influenced by molecular stiffness, while the role of sample annealing and molecular weight remains unclear.

Acknowledgment. L.G.-R. thanks the University of Michigan Rackham School of Graduate Studies and the Alfred P. Sloan Foundation for fellowship support. This work was supported by the National Science Foundation (DMR-9707975, DMR-9510274, and NYI Award DMR-9257569)).

Supporting Information Available: A detailed description of the method used to calculate the local curvature of HRTEM lattice images. This material is available free of charge via the Internet at http://pubs.acs.org.

References and Notes

(1) Safran, S. A. *Adv. Phys.* **1999**, *48*, 395.
(2) Wilson, P. M. Ph.D. Thesis, University of Michigan, 1994.
(3) Lovinger, A. J.; Katz, H. E.; Dodabalapur, A. *Chem. Mater.* **1998**, *10*, 3275.
(4) Salaneck, W. R. *Contemp. Phys.* **1989**, *30*, 403.
(5) Brédas, J. L.; Street, G. B.; Thémans, B.; André, J. M. *J. Chem. Phys.* **1985**, *83*, 1323.
(6) Batchelder, D. N. *Contemp. Phys.* **1998**, *29*, 3.
(7) Inganäs, O. *Trends Polym. Sci.* **1994**, *2*, 189.
(8) Nye, J. F. *Acta Metall.* **1953**, *1*, 153.
(9) Nabarro, F. R. N. *Theory of Crystal Dislocations*; Oxford University Press: New York, 1987.
(10) Srolovitz, D. J.; Safran, S. A.; Tenne, R. *Phys. Rev. E* **1994**, *49*, 5260.
(11) Kübel, C.; González-Ronda, L.; Drummy, L. F.; Martin, D. C. *J. Phys. Org. Chem.* **2000**, *13*, 1.
(12) Martin, D. C.; Berger, L. L.; Gardner, K. H. *Macromolecules* **1991**, *24*, 3921.
(13) Martin, D. C. *Trends Polym. Sci.* **1993**, *1*, 178.
(14) Lovinger, A. J.; Davis, D. D.; Dodabalapur, A.; Katz, H. E.; Torsi, L. *Macromolecules* **1996**, *29*, 4952.
(15) Garnier, F.; Yassar, A.; Hajlaoui, R.; Horowitz, G.; Deloffre, F.; Servet, B.; Ries, S.; Alnot, P. *J. Am. Chem. Soc.* **1993**, *115*, 8716.
(16) Katz, H. E.; Laquindanum, J. G.; Lovinger, A. J. *Chem. Mater.* **1998**, *10*, 633.
(17) Lovinger, A. J.; Davis, D. D.; Dodabalapur, A.; Katz, H. E. *Chem. Mater.* **1996**, *8*, 2836.
(18) Laquindanum, J. G.; Katz, H. E.; Lovinger, A. J. *J. Am. Chem. Soc.* **1998**, *120*, 664.
(19) Dimitrakopoulos, C. D.; Brown, A. R.; Pomp, A. *J. Appl. Phys.* **1996**, *80*, 2501.
(20) Laquindanum, J. G.; Katz, H. E.; Lovinger, A. J.; Dodabalapur, A. *Chem. Mater.* **1996**, *8*, 2542.
(21) Bao, Z.; Lovinger, A. J.; Brown, J. *J. Am. Chem. Soc.* **1998**, *120*, 207.
(22) González-Ronda, L. Ph.D. Thesis, University of Michigan, 2000.
(23) Nanos, J. I.; Kampf, J. W.; Curtis, M. D.; González, L.; Martin, D. C. *Chem. Mater.* **1995**, *7*, 2232.
(24) González-Ronda, L.; Martin, D. C.; Nanos, J. I.; Politis, J. K.; Curtis, M. D. *Macromolecules* **1999**, *32*, 4558.
(25) Politis, J. K.; Curtis, M. D.; González-Ronda, L.; Martin, D. C. *Chem. Mater.* **2000**, *12*, 2798.
(26) González-Ronda, L.; Martin, D. C. *Macromolecules* **1997**, *30*, 1524.
(27) Sethian, J. A. *J. Diff. Geom.* **1989**, *31*, 131.
(28) Gunther, J.; Thomas, E. L.; Clingman, S.; Ober, C. K. *Polymer* **1998**, *39*, 4497.
(29) Tan, Z.; Diao, B.; Berry, G. C. *Macromolecules* **1999**, *32*, 7172.
(30) Martin, D. C.; Thomas, E. L. *Polymer* **1995**, *36*, 1743.
(31) Kumar, S.; Adams, W. W. *Polymer* **1990**, *31*, 15.
(32) Molecular Simulations, Inc. (now Accelrys), Cerius^2 Molecular Modelling Software, Version 3.5, 1998.
(33) Wilson, P. M.; Martin, D. C. *Ultramicroscopy* **1996**, *62*, 215.
(34) Pradere, P.; Thomas, E. L. *Ultramicroscopy* **1990**, *32*, 149.
(35) Martin, D. C.; Thomas, E. L. *Philos. Mag. A* **1991**, *64*, 903.

(36) Srolovitz, D. J.; Safran, S. A.; Homyonfer, M.; Tenne, R. *Phys. Rev. Lett.* **1995**, *74*, 1779.
(37) Politis, J. K.; Somoza, F. B.; Kampf, J. W.; Curtis, M. D.; González Ronda, L.; Martin, D. C. *Chem. Mater.* **1999**, *11*, 2274.
(38) Mandelbrot, B. B. *Fractal Geometry of Nature*; Freeman: New York, 1983.
(39) Courboin, D.; Grouillet, A.; André, E. *Surf. Sci.* **1995**, *342*, L1111.
(40) Buchko, C. J. Ph.D. Thesis, University of Michigan, 1997.
(41) Saariaho, M.; Ikkala, O.; Szleifer, I.; Erukhimovich, I.; ten Brinke, G. *J. Chem. Phys.* **1997**, *107*, 3267.

MA025657E